Spectrochimica Acta Part A: Molecular and Biomolecular Spectroscopy 97 (2012) 811–824

Contents lists available at SciVerse ScienceDirect

Spectrochimica Acta Part A: Molecular and Biomolecular Spectroscopy

journal homepage: www.elsevier.com/locate/saa

Vibrational spectra, UV and NMR, first order hyperpolarizability and HOMO–LUMO analysis of 2-amino-4-chloro-6-methylpyrimidine

T. Jayavarthanan [a], N. Sundaraganesan [b,*], M. Karabacak [c], M. Cinar [c], M. Kurt [d]

[a] Department of Physics (Science and Humanities), Sri Manakula Vinayagar Engineering College, Madagadipet, Puducherry 605107, India
[b] Department of Physics (Engg.), Annamalai University, Annamalai Nagar 608 002, Chidambaram, Tamil Nadu, India
[c] Department of Physics, AfyonKocatepe University, 03040, Afyonkarahisar, Turkey
[d] Department of Physics, Ahi Evran University, 40100 Kırsehir, Turkey

HIGHLIGHTS

- The FTIR and FT-Raman spectra of 2A4Cl6MP were recorded.
- The vibrational frequencies were calculated by DFT method and discussed.
- NMR and UV–Vis spectra were also recorded and compared with calculated ones.

GRAPHICAL ABSTRACT

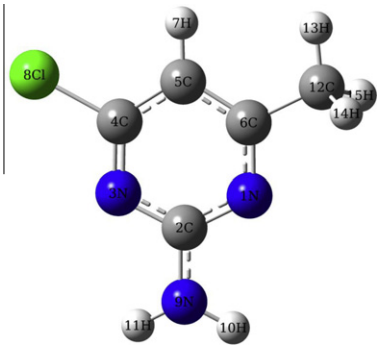

ARTICLE INFO

Article history:
Received 24 May 2012
Received in revised form 12 July 2012
Accepted 13 July 2012
Available online 22 July 2012

Keywords:
TD-DFT
Vibrational spectra
First order hyperpolarizability
NMR
HOMO–LUMO
2-Amino-4-chloro-6-methylpyrimidine

ABSTRACT

The solid phase FTIR and FT–Raman spectra of 2-amino-4-chloro-6-methylpyrimidine (2A4Cl6MP) have been recorded in the regions 400–4000 and 50–4000 cm^{-1}, respectively. The spectra have been interpreted interms of fundamentals modes, combination and overtone bands. The structure of the molecule has been optimized and the structural characteristics have been determined by density functional theory (B3LYP) method with 6-311++G(d,p) as basis set. The vibrational frequencies were calculated and were compared with the experimental frequencies, which yield good agreement between observed and calculated frequencies. The infrared and Raman spectra have also been predicted from the calculated intensities. ^{1}H and ^{13}C NMR spectra were recorded and ^{1}H and ^{13}C nuclear magnetic resonance chemical shifts of the molecule were calculated using the gauge independent atomic orbital (GIAO) method. UV–Vis spectrum of the compound was recorded in the region 200–400 nm and the electronic properties HOMO and LUMO energies were measured by time-dependent TD-DFT approach. Nonlinear optical and thermodynamic properties were interpreted. All the calculated results were compared with the available experimental data of the title molecule.

Introduction

Pyrimidine is one of the parent compounds of a diverse series of heterocyclic compounds, members of which are important components of many natural products and biological systems. A convenient synthetic approach to new biologically active compounds of the pyrimidine series is provided by nucleophilic substitution of halogen atoms or other easily leaving groups in even positions of the ring by pharmacophoric groups. Pyrimidine and its derivatives have good antiinflammatory activity [1]. Pyrimidine derivatives form the basis of a large number of pharmacological products, as inhibitors of HIV-1 integrase [2], anticancer drugs [3] and protein kinase inhibitors [4]. The realization of the biochemical

* Corresponding author. Tel.: +91 9442068405.
E-mail address: sundaraganesan_n2003@yahoo.co.in (N. Sundaraganesan).

1386-1425/$ - see front matter © 2012 Elsevier B.V. All rights reserved.
http://dx.doi.org/10.1016/j.saa.2012.07.064

importance of nucleic acids has occasioned a great revival of interest in the chemistry of pyrimidines. Among them, substituted pyrimidines have become increasingly important as biologically interesting compounds, materials and ligands in molecular recognition [5]. Chlorinated pyrimidine substrates can, for example, be utilised in various palladium catalysed cross-coupling reactions [6] and nucleophilic aromatic substitution processes [7,8].

To the best of our knowledge, neither quantum chemical calculation, nor the vibrational spectra of 2-amino-4-chloro-6-methylpyrimidine (2A4Cl6MP) have been reported. Therefore, the present investigation was undertaken to study the vibrational spectra of this molecule completely and to identify the various modes with greater wavenumber accuracy. Density functional theory (DFT) calculations have been performed to support our wavenumber assignments. The interaction energies, NMR spectral analysis, molecular electrostatic potential, thermodynamic and nonlinear optical properties of the title compound were investigated at the B3LYP/6-311++G(d,p) level.

Experimental details

The 2-amino-4-chloro-6-methylpyrimidine sample was purchased from Sigma–Aldrich Company (USA) with a stated purity 97% and it was used as such without further purification. The sample was prepared using a KBr disc technique because of solid state. The FT-IR spectrum of molecule was recorded in the region 400–4000 cm^{-1} on a Perkin Elmer FT-IR spectrometer calibrated using polystyrene bands. The FT-Raman spectrum of the sample was recorded using 1064 nm line of Nd:YAG laser as excitation wave length in the region 50–4000 cm^{-1} on a Bruker RFS 100/S FT-Raman spectrometer. The detector is a liquid nitrogen cooled Ge detector. Five hundred scans were accumulated at 4 cm^{-1} resolution using a laser power of 100 mW.

The ultraviolet absorption spectra of 2A4Cl6MP dissolved in ethanol are examined in the range 200–400 nm using Shimadzu UV-1800 PC, UV–Vis recording Spectrometer. Data are analyzed by UV PC personal spectroscopy software, version 3.91.

NMR experiments were performed in Bruker DPX 600 MHz at 300 K. The compound was dissolved in DMSO. Chemical shifts were reported in ppm relative to tetramethylsilane (TMS) for ^{1}H, ^{13}C NMR and DEPT 135 spectra. ^{1}H and ^{13}C NMR spectra were obtained at a base frequency of 600 MHz and 150 MHz, respectively.

Computational details

The DFT calculations were performed using the Gaussian 03 program package [9]. The calculations employed the B3LYP exchange-correlation functional, which combines the hybrid functional of Becke [10,11] with the gradient-correlation functional of Lee et al. [12] and the split-valence polarized 6-311++G(d,p) basis set [13]. The harmonic vibrational frequencies were calculated at the same level of theory for the optimized structures. Vibrational band assignments were made using the Gauss-View molecular visualization program [14]. Additionally, the calculated vibrational frequencies were clarified by means of the total energy distribution (TED) analysis and assignments of all the fundamental vibrational modes by using VEDA 4 program [15]. After optimization, ^{1}H and ^{13}C NMR chemical shifts were calculated using the GIAO method [16] in DMSO. UV–Vis spectra, electronic transitions, vertical excitation energies, absorbance and oscillator strengths were computed with the time-dependent DFT method. The electronic properties such as HOMO and LUMO energies were determined by TD-DFT approach. To investigate the reactive sites of the title compound the MEP were evaluated using the B3LYP/6-311++G(d,p) method.

Prediction of Raman intensities

The Raman activities (S_{Ra}) calculated with Gaussian 03 program [9] converted to relative Raman intensities (I_{Ra}) using the following relationship derived from the intensity theory of Raman scattering [17,18],

$$I_i = \frac{f(v_0 - v_i)^4 S_i}{v_i[1 - \exp(-hc\,v_i/kT)]}$$

where; v_0 is the laser exciting wavenumber in cm^{-1} (in this work, we have used the excitation wavenumber v_0 = 9398.5 cm^{-1}, which corresponds to the wavelength of 1064 nm of a Nd:YAG laser), v_i the vibrational wavenumber of the ith normal mode (cm^{-1}), while S_i is the Raman scattering activity of the normal mode v_i. f (is a con-

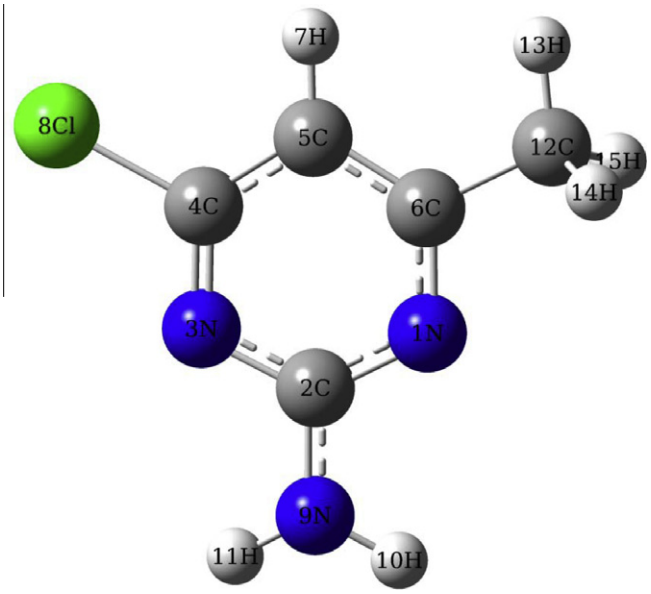

Fig. 1. Optimized molecular structure of 2A4Cl6MP.

Table 1
Comparison of the geometrical parameters of 2A4Cl6MP, bond lengths in angstrom, angles in degrees.

Bond lengths	Exp.[a]	B3LYP	Dihedral angles	B3LYP
N1–C2	1.350	1.340	C6–N1–C2–N3	0.6
N1–C6	1.325	1.338	C6–N1–C2–N9	−178.4
C2–N3	1.343	1.350	C2–N1–C6–C5	−0.2
C2–N9	1.344	1.359	C2–N1–C6–C12	179.9
N3–C4	1.337	1.312	N1–C2–N3–C4	−0.5
C4–C5	1.384	1.392	N9–C2–N3–C4	178.5
C4–Cl8	1.742	1.760	N1–C2–N9–H10	−10.2
C5–C6	1.392	1.397	N1–C2–N9–H11	−170.6
C6–C12	1.544	1.503	N3–C2–N9–H10	170.8
Bond angles			N3–C2–N9–H11	10.3
C2–N1–C6	116.4	116.9	C2–N3–C4–C5	0.1
N1–C2–N3	125.2	126.1	C2–N3–C4–Cl8	179.9
N1–C2–N9	116.6	117.4	N3–C4–C5–C6	0.3
N3–C2–N9	118.2	116.4	Cl8–C4–C5–C6	−179.6
C2–N3–C4	115.5	115.3	C4–C5–C6–N1	−0.2
N3–C4–C5	124.9	124.5	C4–C5–C6–C12	179.7
N3–C4–Cl8	111.7	116.6		
C5–C4–Cl8	123.4	119.0		
C4–C5–C6	113.8	115.5		
N1–C6–C5	124.1	121.7		
N1–C6–C12	119.4	116.7		
C5–C6–C12	116.2	121.6		

[a] Taken from Ref. [19].

Table 2
Comparison of the experimental and calculated vibrational wavenumbers and proposed assignments of 2A4Cl6MP.

No	Experimental wavenumbers		B3LYP/6-311++G(d,p)					TED and assignments
	FT-IR	FT-Raman	Unscaled	Scaled	I_{IR}[a]	SA_{Raman}[b]	[c]IRaman	Assignments
1	3410ms		3745	3588	60.27	47.98	10.41	υ_{asym} NH_2 (100)
2	3318s		3614	3463	97.19	179.12	43.82	υ_{sym} NH_2 (100)
3	3198ms	3192w	3228	3092	0.10	73.88	25.80	υCH (99)
4	2998vw	3098w	3123	2992	14.85	59.65	21.77	υ_{asym} CH_3 (100)
5	2930vw	2996w	3096	2966	7.13	87.15	34.34	υ_{asym} CH_3 (100)
6		2932s	3039	2911	10.11	240.76	100.01	υ_{sym} CH_3 (100)
	2795vw							(1434 + 1371)
	2716vw							(3 × 911)
	2660vw							((2 × 1796) − 962)
	2360w							(2 × 1157)
	2343vw							(3198–875)
7	1638/1653s	1638ms	1638	1610	649.37	13.51	21.08	ρ NH_2 (59) + υ C–NH_2 (18)
8	1579vs	1585w	1611	1583	179.75	11.67	18.78	υ CN (53) + υ CC (18) + ρNH_2 (16)
9	1554vs	1553w	1581	1554	355.34	3.95	6.57	υ CC (40) + υ CN (23)
10	1478s	1468w	1485	1460	145.31	11.09	20.60	ρ CH_2 of CH_3 (40) + β CH of CH_3 (31)
11			1476	1451	8.31	8.03	15.06	ρ CH_2 of CH_3 (55) + β CH of CH_3 (36)
12			1470	1445	26.18	1.23	2.33	υ CN (22) + υ C–NH_2 (20) + ρ NH_2 (14) + ρ CH_2 of CH_3 (9)
13	1434w	1436w	1461	1436	52.46	1.67	3.19	υ CN (32) + υ C–NH_2 (18) + β CH (16) + β NH of NH_2 (12)
14	1371w	1374w	1407	1383	10.30	8.81	18.63	CH_3 umbrella (91)
15	1290/1305ms	1309w	1315	1293	108.13	8.88	20.23	Ring breathing (81)
16	1240w	1251w	1273	1252	19.03	0.73	1.75	Ring deformation (94)
17	1157w		1177	1157	32.07	3.34	9.09	β CH (49) + r NH_2 (16) + υ CC (13)
18	1083w		1100	1081	0.71	0.25	0.76	υ C–CH_3 (23) + r NH_2 (21) + υ CC (16) + υ C–NH_2 (10)
19	1032w		1055	1037	4.32	0.22	0.71	t CH_2 of CH_3 (61) + γ N<u>C</u>CH (36)
20			1028	1011	26.14	0.09	0.29	r NH_2 (31) + υ CN (18) + β CH of CH_3 (10)
21	995w	997m	1013	996	8.12	12.53	42.84	β CCC (35) + r CH_3 (22) + β CCN (13)
22	952w	956s	974	957	1.23	12.69	46.03	υ CN (56) + r CH_3 (11)
23	875s	879w	875	860	96.44	2.17	9.18	β (CCN + NCN) (67) + υ C–CH_3 (16)
24	805w		817	803	20.21	0.87	4.04	γ CH (90)
25	783ms	790w	802	789	8.77	0.11	0.54	γ CN<u>C</u>N (54) + γ CC<u>N</u>C (35)
26	658w		666	654	2.51	0.13	0.81	γ (CC<u>C</u>N + CC<u>N</u>C) (80)
27	610w	610vs	617	606	7.66	12.59	86.04	β (CCN + CNC + NCN) (87)
28	573w	571s	584	574	0.40	0.81	5.96	γ CN<u>C</u>C (80)
29	544w	549vw	547	538	3.63	5.00	40.02	β (CCN + CNC + NCN) (92)
30	523w	523vw	531	522	1.30	0.47	3.95	ωNH_2 (89)
31	494w		497	489	5.58	0.42	3.78	β NCN (31) + r NH_2 (23) + β (CC–CH_3 + NC–CH_3) (20) + β (CN–Cl + NC–Cl) (17)
32	419w	423vs	411	404	6.29	9.87	116.12	υ C–Cl (55) + β (CCN + CNC) (27)
33		324s	300	295	7.14	2.82	51.51	r CH3 (41) + r NH_2 (35)
34		247ms	237	233	0.17	1.67	43.12	β C–Cl (66) + r CH_3 (16)
35		217s	233	229	263.20	1.9	50.35	t NH_2 (97)
36			213	209	0.24	0.47	14.30	γ C–CH_3 (43) + γ CC<u>N</u>C (35)
37		172w	190	186	1.89	0.11	4.01	γ NC<u>N</u>H (72) + γ CC<u>N</u>C (26)
38			152	150	1.50	0.84	43.32	γ NC<u>C</u>C (54) + γ NC<u>N</u>C (30) + γ C–CH_3 (16)
39		81vs	74	72	0.25	0.28	51.42	τ CH_3 (95)

ν_{sym}–ν_{asym}; symmetric–asymmetric stretching, β; in plane bending, γ; out of plane bending, ρ; scissoring, ω; wagging, t; twisting, r; rocking, τ; torsion. [frequency (cm^{-1}).
[a] I_{IR} (K $mmol^{-1}$), IR intensities.
[b] SA_{Raman} ($Å^4$ amu^{-1})], Raman scattering activities.
[c] I_{Raman} (Arb. units) Raman intensities. The out-of-plane bonded atoms were underlined in the last column.

stant equal to 10^{-12}) is a suitably chosen common normalization factor for all peak intensities. *h, k, c* and *T* are Planck and Boltzmann constants, speed of light and temperature in Kelvin, respectively.

Results and discussion

Molecular structure

The first task for the computational work is to determine the optimized geometries of the studied molecule. The optimized molecular structure of 2-amino-4-chloro-6-methylpyrimidine (2A4Cl6MP) with the numbering scheme of the atoms obtained from Gauss view program [14] is shown in Fig. 1. The optimized structural parameters such as bond lengths, bond angles and dihedral angles of 2A4Cl6MP molecule are determined by B3LYP level with 6-311++G(d,p) as basis set were compared with closely related experimental parameters obtained from the X-ray diffraction studies [19] shown in Table 1.

The 2A4Cl6MP is heterocyclic molecule and a resonance effect is observed in the ring of this molecule. As a result, C—C bond lengths and C—C—C bond angle in the six member ring are similar to the benzene molecule. In the benzene ring, C—C bond length is about 1.396 Å [20], our calculations were similar to this value, for example the optimized bond length of C—C in phenyl ring fall in the range 1.392–1.397 Å by B3LYP/6-311++G(d,p) level, show good agreement with experimental data of 1.384–1.392 Å. Ourselves have predicted both C=N bond lengths of 2,4,6-triaminopyrimidine as 1.339 and 1.325 Å by B3LYP and HF method, respectively. However, on comparing with experimental data [19], both C=N bond lengths of 2A4Cl6MP are differed by 0.008 Å at B3LYP/6-311++G(d,p) method. Our optimized C—Cl bond length of 1.503 Å is shorter by about 0.041 Å when compared with experimental data of 1.544 Å. The amino group orients with the pyrimidine ring

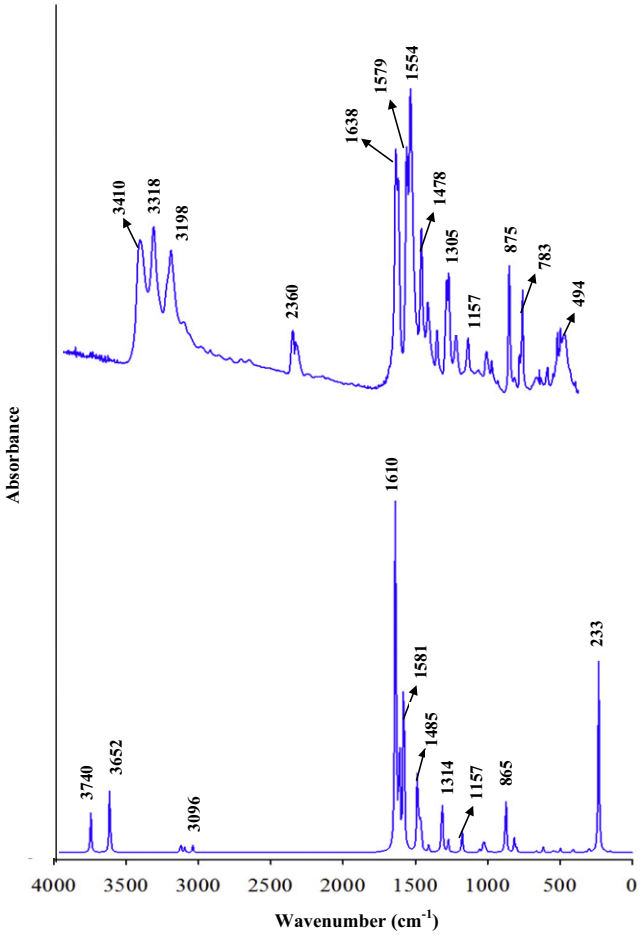

Fig. 2. Experimental (top) and theoretical (bottom) FTIR spectra of 2A4Cl6MP.

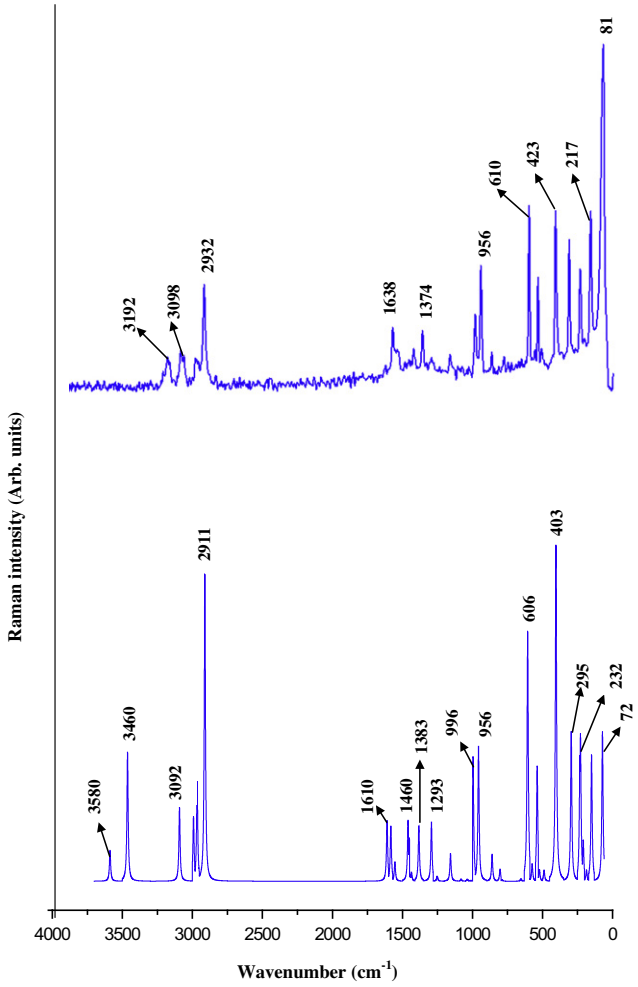

Fig. 3. Experimental (top) and theoretical (bottom) FT-Raman spectra of 2A4Cl6MP.

N9–C2–N3–C4 at 178.5°, the chloro group orients with pyrimidine ring C2–N3–C4–Cl8 at 179.9° and methyl group orients with pyrimidine ring C2–N1–C6–C12 at 179.9° suggesting that the title molecule was planar as evident from the above dihedral angles. From the theoretical results of our title molecule, we find that most of the optimized bond lengths and angles are slightly smaller as well as longer than the experimental value, this is due to the fact that the theoretical calculations belong to isolated molecule in gaseous phase and experimental results belong to molecule in solid state.

Vibrational assignments

The vibrational spectrum is mainly determined by the modes of free molecule observed at higher wavenumbers, together with the lattice (translational and vibrational) modes in the low wavenumber region. In our present study, we have performed a frequency calculation analysis to obtain the spectroscopic signature of 2-amino-4-chloro-6-methylpyrimidine. The 2A4Cl6MP molecule consists of 15 atoms therefore they have 39 vibrational normal modes. All the frequencies are assigned in terms of fundamental, overtone and combination bands. Assignments have been made on the basis of relative intensities, energies, line shape and total energy distribution (TED). The measured (FTIR and FT-Raman) wavenumbers and assigned wavenumbers of the some selected intense vibrational modes calculated at the B3LYP level using basis set 6-311++G(d,p) along with their TED are given in Table 2. For B3LYP with 6-311++G(d,p) basis set, the wavenumbers in the ranges from 4000 to 1700 cm^{-1} and lower than 1700 cm^{-1} are scaled with 0.958 and 0.983, respectively [21]. The calculated Raman and IR intensities were used to convolute each predicted vibrational mode with a Lorentzian line shape with a full width at half maximum (FWHM = 10 cm^{-1}) to produce simulated spectra. This reveals good correspondence between theory and experiment in main spectral features. The experimental and theoretical FTIR and FT-Raman spectra are shown in Figs. 2 and 3.

NH_2 vibrations

The amino and methylene groups are generally referred to as electron donating substituents in aromatic ring system [22]. The CH_2 interacts with nearby π-system via hyperconjugation, while the NH_2 share its lone pair of electrons with the π-electrons in a ring. Both mechanisms imply electronic delocalization and are taken into account by the molecular orbital approach. The molecule under investigation possesses one NH_2 group and hence one can expect one asymmetric and one symmetric N–H stretching vibrations. It is stated that in amines, the N–H stretching vibrations occur in the region 3500–3300 cm^{-1}. The NH_2 asymmetric and symmetric stretching vibration in FTIR spectrum found at 3414 cm^{-1} and 3312 cm^{-1}, respectively for 2-amino-4,6-dimethoxy pyrimidine molecule [23]. For the same vibration the FT-Raman band was observed at 3418 and 3311 cm^{-1}. In our title molecule the asymmetric NH_2 stretching vibrations appears at 3410 and the symmetric stretching vibration appears at 3318 cm^{-1}. The antisymmetric (ν_{as}) stretching mode is calculated at the higher wavenumber 3588 cm^{-1} than the symmetric (ν_s) one at 3463 cm^{-1} by B3LYP/6-

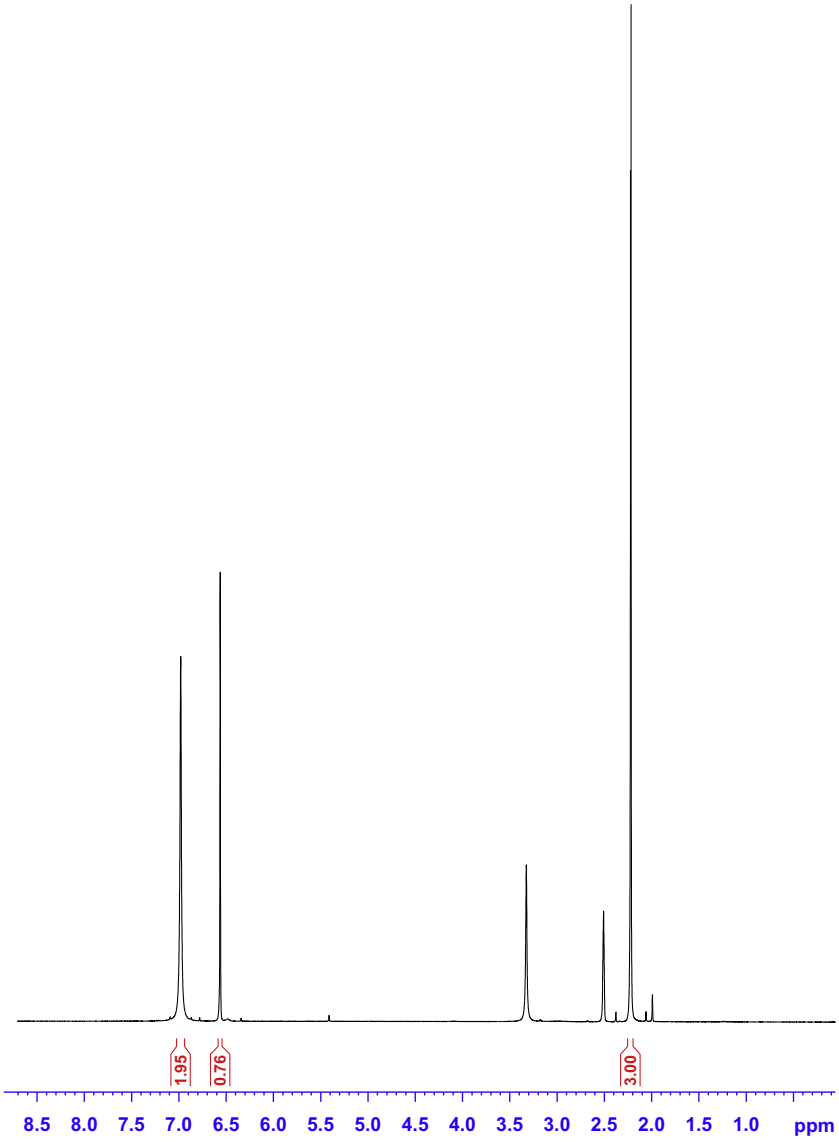

Fig. 4. ^{1}H NMR spectrum of 2A4Cl6MP.

311++G(d,p) level having mode Nos. 1 and 2 in Table 2. The last column of TED of vibration shows that it is pure modes contributing 100%, as it is evident from the Table 2.

The scissoring mode of NH_2 group appears in the region 1615–1650 cm^{-1} in benzene derivatives with NH_2 substituents [24,25]. For 2,4-diamino-6-hydroxy-5-nitraso-pyrimidine [26], the FT-Raman band at 1664 cm^{-1} was assigned to NH_2 scissoring mode. In our title molecule, the calculated frequency for the scissoring mode of NH_2 is at 1610 cm^{-1} and 1583 cm^{-1} (mode Nos. 7 and 8). This mode (mode Nos. 7 and 8) is also coupled with ring stretching mode as shown in Table 2. The computed vibrations well coincide with the experimental (1638, 1579 cm^{-1} in FTIR and 1638 and 1585 cm^{-1} in FT-Raman).

The in-plane bending $–NH_2$ rocking and out-of-plane wagging vibrations are also assigned in the expected range. The amino in-plane bending rocking mode appears in the range 1150–900 cm^{-1} while the wagging bands between 850 and 500 cm^{-1}. Therefore, the predicted wavenumbers at 1011 and 522 cm^{-1} are attributed to the amino rocking and wagging modes, respectively. These amino vibrations are also in good agreement with literature values of aniline [27].

C–Cl vibrations

The aliphatic C—Cl bands absorb [22] at 830–560 cm^{-1} and the substitution of more than one chlorine on a carbon atom raises the C—Cl wavenuber. The C—Cl stretching mode is reported at around 738 cm^{-1} for dichloromethane and scissoring mode δC—Cl at around 284 cm^{-1} [22]. Pazderza et al. [28,29] reported C—Cl stretching mode at 890 cm^{-1}. Arslan et al. [30] reported *ν*C—Cl at 683 cm^{-1} (experimentally) and 711, 736, 687, 697 cm^{-1} theoretically. Wojciechowski and Michalska [31] reported the C—Cl stretching vibration at 379 cm^{-1} in both IR and Raman spectra of 4-chloroaniline. In our title molecule, the C—Cl stretching frequency appears in FTIR at 419 cm^{-1} and in FT-Raman at 423 cm^{-1}. The unscaled wavenumber at 411 cm^{-1} (mode No. 32) shows good correlation when compared with experimental counterpart. According to Table 2, the TED for the C—Cl stretching vibration indicates that this mode is a coupled one.

Ring vibrations

For the parasubstituted benzene ring, the C—C ring stretching modes are observed at 1590, 1474, 1395, 1308 and 1232 cm^{-1} (IR), 1599, 1574, 1489, 1406 and 1310 cm^{-1} (Raman) an 1589,

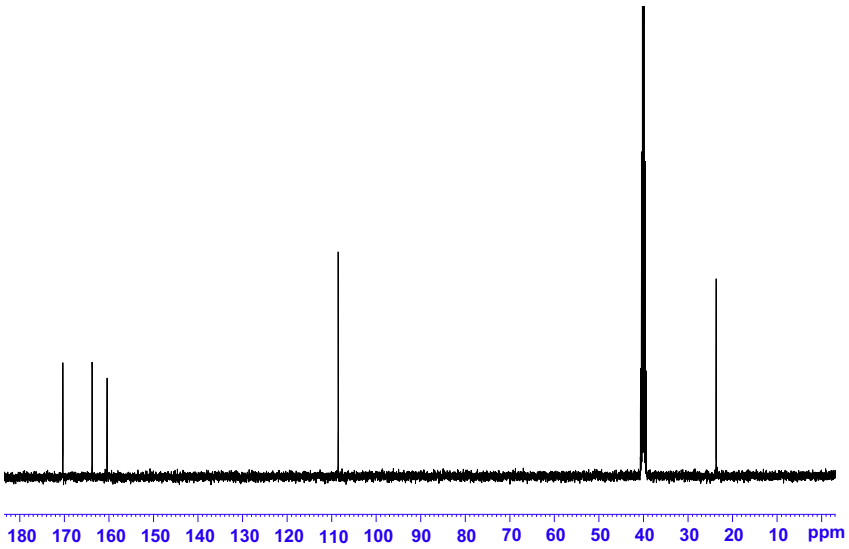

Fig. 5. ^{13}C NMR spectrum of 2A4Cl6MP.

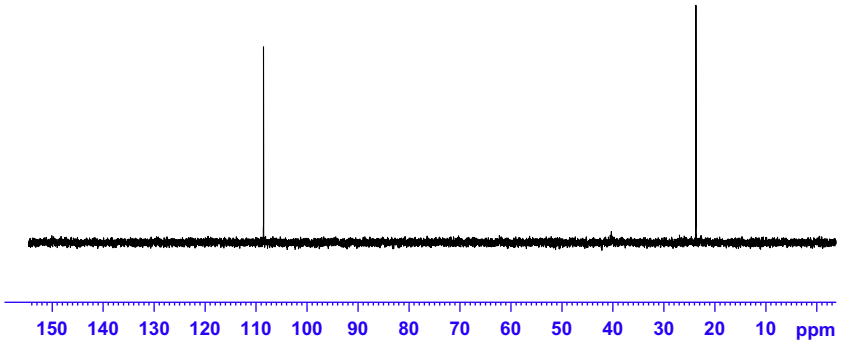

Fig. 6. DEPT 135 NMR spectrum of 2A4Cl6MP.

Table 3
The observed (in $CDCl_3$) and predicted ^1H and ^{13}C NMR isotropic chemical shifts (with respect to TMS, all values in ppm) for 2A4Cl6MP.

Atom	Experimental	Theoretical		Atom	Experimental	Theoretical	
	DMSO	Gas	DMSO		DMSO	Gas	DMSO
H7	6.98	6.06	6.35	C2	160.4	162.7	163.9
H10	6.56	4.26	4.74	C4	163.7	171.4	171.3
H11	6.56	4.21	4.64	C5	108.5	108.6	109.5
H13	2.22	1.54	1.88	C6	170.3	171.5	174.7
H14	2.22	2.10	2.21	C12	23.7	20.7	21.4
H15	2.22	2.08	2.20				

1578, 1478, 1384, 1300 and 1229 cm^{-1} theoretically [22,32]. The C—C ring stretching mode of 2A4Cl6MP appears in our calculations at 1554 cm^{-1} (mode No. 9) and it contributes 40% TED with minor contribution of 23% υCN. The other C—C ring stretching mode appears at higher frequency of 1583 cm^{-1} with 18% TED contribution. The TED of these assignments predicts that they are mixed modes with some contribution of νC–N vibration.

Primary aromatic amines with nitrogen directly on the ring absorb at 1330–1260 cm^{-1} due to stretching of the phenyl carbon–nitrogen bond [30,22]. Sandhyarani et al. [33] reported νC–N at 1332 cm^{-1}, Anto et al. [34] and Ambujakshan et al. [35] reported νC–N at 1332 cm^{-1}, 1331 cm^{-1} (IR), 1315 cm^{-1} (Raman) 1315 and 1323 cm^{-1} (HF). In the case of 2,4,6-triaminopyrimidine, the band observed in the range 1430–1575 cm^{-1} in both FTIR and Raman spectra had been assigned to C—N, C═N stretching vibrations, respectively [36]. The theoretically computed values of C—N and C═N stretching vibrations are found in the range 1457–1558 cm^{-1}. For our title molecule 2A4Cl6MP, the DFT calculations give the νC–N mode at 1583, 1554, 1445, 1436 cm^{-1} and 957 cm^{-1} and at 1585, 1553, 1436 and 956 cm^{-1} in FT-Raman spectrum. In our calculations, this mode is a mixed mode as it is evident from TED calculations.

Methyl group vibrations

The title molecule 2A4Cl6MP possesses a CH_3 group in the sixth position. For the assignments of CH_3 group frequencies, one can expect nine fundamentals to be associated to each CH_3 group, namely the symmetrical stretching in CH_3 (CH_3 sym.stretch) and asymmetrical stretching (CH_3 asy.stretch), in-plane stretching modes (i.e. in plane hydrogen stretching mode); the symmetrical (CH_3 sym. deform) and asymmetrical (CH_3 asy deform) deformation modes; the in-plane rocking (CH_3 ipr), out-of-plane rocking (CH_3 opr) and twisting (t CH_3) bending modes. The C—H stretching vibration in CH_3 occurs at lower frequencies than those of aromatic ring (3000–3100 cm^{-1}).

The asymmetric C—H stretching mode of CH_3 group is expected around 2980 cm^{-1} and the symmetric [37,38] one is expected in the region 2870 cm^{-1}. For 2A4Cl6MP, the CH_3 stretching vibration around 3100–2900 cm^{-1}, the in-plane deformation around 1450–1370 cm^{-1} and the rocking around 1040–990 cm^{-1} [39]. The calculated and observed wavenumbers of asymmetric and symmetric

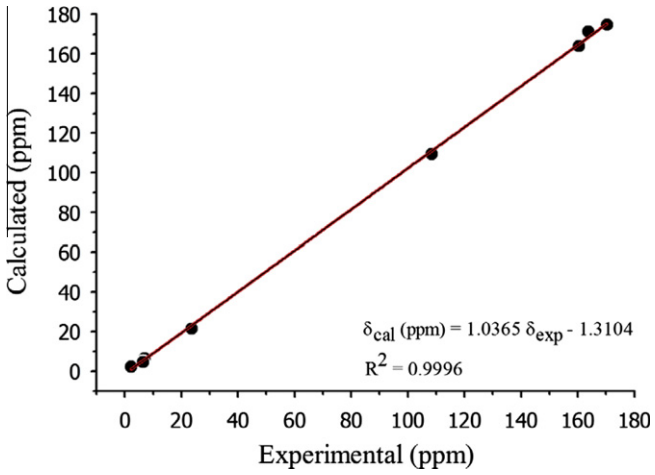

Fig. 7. Correlation graphic of carbon NMR chemical shifts for 2A4Cl6MP.

Table 4
The electric dipole moment, polarizability and first order hyperpolarizability of 2A4Cl6MP.

	a.u.	esu ($\times10^{-24}$)		a.u.	esu ($\times10^{-33}$)
α_{xx}	120.9362	17.9227	β_{xxx}	−247.5983	−2139.0762
α_{xy}	−2.7645	−0.4097	β_{xxy}	10.2989	88.9750
α_{yy}	111.0464	16.4571	β_{xyy}	191.0954	1650.9308
α_{xz}	−5.4970	−0.8147	β_{yyy}	−238.7868	−2062.9506
α_{yz}	3.2277	0.4783	β_{xxz}	14.4958	125.2336
α_{zz}	56.9477	8.4396	β_{xyz}	12.2597	105.9152
α_{tot}	96.3101	14.2732	β_{yyz}	−33.3703	−288.2957
$\Delta\alpha$	217.7985	32.2777	β_{xzz}	−27.2192	−235.1550
μ_x	−0.8596		β_{yzz}	−7.4433	−64.3047
μ_y	−0.0990		β_{zzz}	3.8294	33.0833
μ_z	−0.0961		β_x	−83.7221	−723.3004
μ	0.8706		β_y	−235.9312	−2038.2802
			β_z	−15.0451	−129.9788
			β_{tot}	250.7973	2166.7128

stretching vibrations of CH_3 group are listed in Table 2. The CH_3 stretching vibrations are contributing exactly 100% of TED.

For the methyl substituted benzene drerivatives, the asymmetric and symmetric deformation vibrations of CH_3 group normally appear in the region 1465–1440 cm^{-1} and 1390–1370 cm^{-1}, respectively [39–41]. The wavenumbers of the modes involving CH_3 deformation vibrations agree with commonly accepted regions of these vibrations [39,42]. The CH_3 torsional mode is expected below 400 cm^{-1}, the computed bands at 72 cm^{-1} in 2A4Cl6MP is assigned to this mode, the spectral measurements in FT-Raman spectrum at 81 cm^{-1} show good correlation with computed wavenumber.

^{13}C and ^{1}H NMR spectral analysis

The relations between the calculated and experimental chemical shifts are linear and described by the following equation:

$$\delta_{cal.}\ (ppm) = 1.0365\ \delta_{exp.} - 1.3104 \qquad (R^2 = 0.9996)$$
$$^{1}H:\ \delta_{cal.}\ (ppm) = 0.7150\ \delta_{exp.} + 0.4810 \qquad (R^2 = 0.9217)$$
$$^{13}C:\ \delta_{cal.}\ (ppm) = 1.0541\ \delta_{exp.} - 3.9364 \qquad (R^2 = 0.9994)$$

The performances of the B3LYP method with respect to the prediction of the chemical shifts within the molecule were quite close. However, ^{13}C NMR calculations gave a slightly better coefficient and lower standard error (R^2 = 0.9994) than for ^{1}H NMR chemical shifts (R^2 = 0.9217). The measured ^{13}C, ^{1}H and DEPT NMR spectra are shown in Figs. 4–6. The computed and experimental ^{13}C NMR and ^{1}H NMR chemical shifts are tabulated in Table 3. The correlations between the experimental and calculated chemical shifts obtained by DFT/B3LYP method are shown in Fig. 7. As can be seen from Table 3 and Fig. 7, there is a good agreement between experimental and theoretical chemical shift results for the title compound. Aromatic carbons give signals in overlapped areas of the spectrum with chemical shift values from 100 to 150 ppm [43,44]. In our present investigation, the experimental chemical shift values of aromatic carbons are in the range 108.5–170.3 ppm. As can be seen from Table 3, the calculated values show moderate agreement with measured values except the ^{1}H NMR chemical shifts of the active hydrogen atoms H10, H11 and H13 due to the influence of rapid proton exchange, hydrogen bond, solvent effect, etc. in the molecular system. The experimental chemical shift value of C6 atom is more diverged from the literature value due to the substitution of methyl group. The theoretically calculated chemical shifts of C4 atom is found at 171.3 in DMSO solvent, which is largely downfield relative to aromatic benzene [45] due to the electronegative Cl atom which decrease the electron density of the adjacent carbon atoms of the ring. The methyl groups are generally denoted as electron donating groups, so they will be more shielded. The methyl carbon C12 atom appeared at 23.7 ppm, the computed chemical shift values at 20.7 and 21.4 ppm are assigned to the methyl carbon atom C12 in gas phase and DMSO solvent, respectively.

Nonlinear optical effects

Nonlinear optical (NLO) effects arise from the interactions of electromagnetic fields in various media to produce new fields altered in phase, frequency, amplitude or other propagation characteristics from the incident fields [46]. NLO is at the forefront of current research because of its importance in providing the key functions of frequency shifting, optical modulation, optical switching, optical logic, and optical memory for the emerging technologies in areas such as telecommunications, signal processing, and optical interconnections [47–50].

The first hyperpolarizability (β_0) of this novel molecular system, and related properties (β, α_0 and $\Delta\alpha$) of 2A4Cl6MP are calculated using B3LYP/6-311++G(d,p) method, based on the finite-field approach. In the presence of an applied electric field, the energy of a system is a function of the electric field. First order hyperpolarizability is a third rank tensor that can be described by $3 \times 3 \times 3$ matrices. The 27 components of the 3D matrix can be reduced to 10 components due to the Kleinman symmetry [51]. It can be given in the lower tetrahedral format. It is obvious that the lower part of the $3 \times 3 \times 3$ matrices is a tetrahedral. The components of β are defined as the coefficients in the Taylor series expansion of the energy in the external electric field. When the external electric field is weak and homogeneous, this expansion becomes:

$$E = E^0 - \mu_\alpha F_\alpha - 1/2\alpha_{\alpha\beta}F_\alpha F_\beta - 1/6\beta_{\alpha\beta\gamma}F_\alpha F_\beta F_\gamma + \cdots.$$

where E^0 is the energy of the unperturbed molecules, F_α is the field at the origin, μ_α, $\alpha_\alpha\beta$ and $\beta_{\alpha\beta}\gamma$ are the components of dipole moment, polarizability and the first order hyperpolarizabilities, respectively. The total static dipole moment μ, the mean polarizability α_0, the anisotropy of the polarizability $\Delta\alpha$ and the mean first order hyperpolarizability β_0, using the x, y, z components they are defined as:

$$\mu = \left(\mu_x^2 + \mu_y^2 + \mu_z^2\right)^{1/2}$$
$$\alpha_0 = (\alpha_{xx} + \alpha_{yy} + \alpha_{zz})/3$$
$$\alpha = 2^{-1/2}\left[(\alpha_{xx} - \alpha_{yy})^2 + (\alpha_{yy} - \alpha_{zz})^2 + (\alpha_{zz} - \alpha_{xx})^2 + 6\alpha_{xx}^2\right]^{1/2}$$
$$\beta_0 = \left(\beta_x^2 + \beta_y^2 + \beta_z^2\right)^{1/2}$$

Table 5
Second order perturbation theory analysis of Fock matrix in NBO basis for 2A4Cl6MP (DFT/B3LYP/6-311++G(d,p).

Donor (*i*)	Type of bond	Occupancy	Acceptor (*j*)	Type of bond	Occupancy	$E(2)$ (kJ mol^{-1})[a]	$E(j)-E(i)$ (a.u.)[b]	$F(i,j)$ (a.u.)[c]
N1–C2	σ	1.98359	N1–C6	σ*	0.02134	1.16	1.37	0.036
			C2–N3	σ*	0.04255	1.49	1.33	0.040
			C2–N9	σ*	0.03352	1.06	1.30	0.033
			C6–C12	σ*	0.02087	3.78	1.25	0.061
			N9–H11	σ*	0.00630	1.71	1.26	0.041
	π	1.69309	N3–C4	π*	0.43693	7.74	0.29	0.044
			C5–C6	π*	0.32762	35.1	0.33	0.096
N1–C6	σ	1.98269	N1–C2	σ*	0.03703	1.18	1.35	0.036
			C2–N9	σ*	0.03352	3.62	1.30	0.061
			C5–C6	σ*	0.03504	1.80	1.40	0.045
			C5–H7	σ*	0.01324	1.58	1.27	0.040
			C6–C12	σ*	0.02087	0.93	1.25	0.030
			C12–H13	σ*	0.00406	0.63	1.24	0.025
C2–N3	σ	1.97337	N1–C2	σ*	0.03703	1.46	1.35	0.040
			C2–N9	σ*	0.03352	0.82	1.29	0.029
			N3–C4	σ*	0.02761	1.44	1.38	0.040
			C4–Cl8	σ*	0.06331	5.97	0.96	0.068
			N9–H10	σ*	0.00638	1.75	1.25	0.042
C2–N9	σ	1.99028	N1–C2	σ*	0.03703	1.03	1.36	0.034
			N1–C6	σ*	0.02134	2.25	1.38	0.050
			C2–N3	σ*	0.04255	0.80	1.34	0.030
			N3–C4	σ*	0.02761	2.13	1.40	0.049
N3–C4	σ	1.98664	C2–N3	σ*	0.04255	1.27	1.38	0.038
			C2–N9	σ*	0.03352	3.17	1.35	0.059
			C4–C5	σ*	0.03653	2.39	1.44	0.053
			C5–H7	σ*	0.01324	1.33	1.32	0.037
N3–C4	π		N1–C2	π*	0.44876	30.2	0.32	0.094
			C5–C6	π*	0.32762	7.62	0.35	0.047
C4–C5	σ	1.98203	N3–C4	σ*	0.02761	2.52	1.29	0.051
			C5–C6	σ*	0.03504	2.69	1.31	0.053
			C5–H7	σ*	0.01324	1.57	1.18	0.038
			C6–C12	σ*	0.02087	3.84	1.15	0.06
C4–Cl8	σ	1.98618	C2–N3	σ*	0.04255	2.95	1.21	0.054
			C5–C6	σ*	0.03504	2.14	1.27	0.047
C5–C6	σ	1.97116	N1–C6	σ*	0.02134	1.71	1.25	0.041
			C4–C5	σ*	0.03653	3.37	1.27	0.058
			C4–Cl8	σ*	0.06331	5.49	0.85	0.061
			C5–H7	σ*	0.01324	1.39	1.15	0.036
			C6–C12	σ*	0.02087	1.62	1.13	0.038
C5–C6	π	1.63959	N1–C2	π*	0.44876	10.83	0.26	0.048
			N3–C4	π*	0.43693	37.96	0.25	0.089
			C5–C6	π*	0.32762	1.96	0.28	0.021
			C12–H14	π*	0.00685	2.14	0.66	0.037
			C12–H15	π*	0.00682	2.11	0.66	0.037
C5–H7	σ	1.97688	N1–C6	σ*	0.02134	4.91	1.07	0.065
			N3–C4	σ*	0.02761	5.05	1.09	0.066
			C4–C5	σ*	0.03653	1.34	1.08	0.034
			C5–C6	σ*	0.03504	1.49	1.10	0.036
C6–C12	σ	1.98188	N1–C2	σ*	0.03703	3.28	1.16	0.055
			N1–C6	σ*	0.02134	1.06	1.18	0.032
			C4–C5	σ*	0.03653	2.02	1.19	0.044
			C5–C6	σ*	0.03504	1.62	1.21	0.040
			C12–H14	σ*	0.00685	0.54	1.04	0.021
			C12–H15	σ*	0.00682	0.54	1.04	0.021
N9–H10	σ	1.98838	C2–N3	σ*	0.04255	4.32	1.17	0.064
N9–H11	σ	1.98861	N1–C2	σ*	0.03703	4.45	1.19	0.065
C12–H13	σ	1.98845	N1–C6	σ*	0.02134	4.80	1.05	0.063
C12–H14	σ	1.97355	C5–C6	σ*	0.03504	2.06	1.07	0.042
			C5–C6	π*	0.32762	4.09	0.52	0.045
C12–H15	σ	1.97369	C5–C6	σ*	0.03504	2.09	1.07	0.042
			C5–C6	π*	0.32762	4.05	0.52	0.045
N1	σ L(1)	1.91213	C2–N3	σ*	0.04255	12.58	0.84	0.093
N3	σ L(1)	1.89445	N1–C2	σ*	0.03703	11.57	0.87	0.091
Cl8	σ L(3)	1.90942	N3–C4	π*	0.43693	16.34	0.30	0.069
N9	σ L(1)	1.76477	N1–C2	π*	0.44876	50.81	0.26	0.110
N1–C2	π*	1.69309	C5–C6	π*	0.32762	105.13	0.03	0.076
N3–C4	π	1.78325	C5–C6	π*	0.32762	91.48	0.03	0.079

[a] $E(2)$ means energy of hyper conjugative interaction (stabilization energy).
[b] Energy difference between donor and acceptor *i* and *j* NBO orbitals.
[c] $F(i,j)$ is the Fock matrix element between *i* and *j* NBO orbitals.

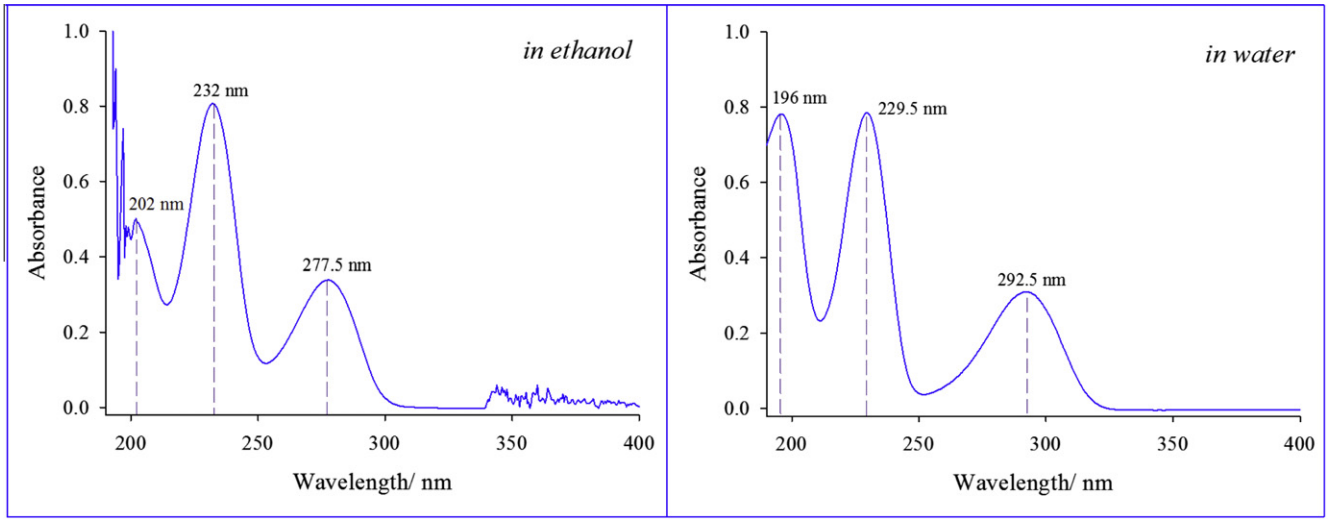

Fig. 8. Experimental UV spectra of 2A4Cl6MP.

and

$$\beta_x = \beta_{xxx} + \beta_{xyy} + \beta_{xzz}$$
$$\beta_y = \beta_{yyy} + \beta_{xxy} + \beta_{yzz}$$
$$\beta_z = \beta_{zzz} + \beta_{xxz} + \beta_{yyz}$$

Table 6
Theoretical and experimental electronic absorption spectra values of 2A4Cl6MP.

Experimental			TD-DFT/6-311++G(d,p)		
Ethanol			Ethanol		
λ (nm)	Abs.	E (eV)	λ (nm)	*E* (eV)	*f*
277.5	0.613	4.4685	272.97 (37 → 38)	4.5420	0.1005
			260.36 (36 → 38)	4.7621	0.0063
232.0	1.458	5.3448	222.69 (36 → 39)	5.5677	0.0002
			218.53 (37 → 39)	5.6737	0.2909
			216.62 (37 → 40)	5.7236	0.024
202.0	0.905	6.1386	208.20 (37 → 41)	5.9549	0.0001
Water			Water		
292.50	0.311	4.2393	273.05 (37 → 38)	4.5407	0.0990
			260.08 (36 → 38)	4.7672	0.0062
229.50	0.785	5.4031	222.38 (36 → 39)	5.5752	0.0002
			218.30 (37 → 39)	5.6796	0.2874
			216.47 (37 → 40)	5.7276	0.0223
196.0	0.782	6.3265	208.37 (37 → 41)	5.9501	0.0001
			Gas		
			266.60 (37 → 38)	4.6505	0.0784
			264.30 (36 → 38)	4.6911	0.0052
			228.42 (36 → 39)	5.4280	0.0000
			222.29 (37 → 40)	5.5775	0.0168
			215.35 (37 → 39)	5.7574	0.1945
			208.28 (37 → 41)	5.9527	0.0028

Since the values of the polarizabilities (α) and hyperpolarizability (β) of the GAUSSIAN 03 output are reported in atomic units (a.u.), the calculated values have been converted into electrostatic units (esu) (α : 1 a.u. = 0.1482×10^{-24} esu; β : 1 a.u. = 8.639×10^{-33} esu).

Urea is one of the prototypical molecules used in the study of the NLO properties of molecular systems. Therefore it was used frequently as a threshold value for comparative purposes. The total molecular dipole moment and first order hyperpolarizability are 0.8706 Debye and 2.1667×10^{-30} esu, respectively and are depicted in Table 4. Total dipole moment of title molecule is approximately one and half times lesser than that of urea and first order hyperpolarizability is 5 times greater than that of urea (μ and β of urea are 1.3732 Debye and 0.3728×10^{-30} cm^5/esu obtained by HF/6-311G(d,p) method [52]). These results indicate that the title compound is a good candidate of NLO material.

To understand this phenomenon in the context of molecular orbital theory, we examined the molecular HOMOs and molecular LUMOs of the title compound. When we see the first hyperpolarizability value, there is an inverse relationship between first hyperpolarizability and HOMO–LUMO gap, allowing the molecular orbitals to overlap to have a proper electronic communication conjugation, which is a marker of the intramolecular charge transfer from the electron donating group through the π-conjugation system to the electron accepting group [53,54].

NBO analysis

By using second-order perturbation theory we investigated the intra and intermolecular interactions, the stabilization energies of the title compound. NBO analysis has been performed on 2A4Cl6MP in order to elucidate intramolecular hydrogen bonding, intramolecular charge transfer (ICT) interactions and delocalization of π-electrons of the pyrimidine ring. The change in electron density (ED) in the (σ*, π*) antibonding orbitals and *E*(2) energies have been calculated by natural bond orbital (NBO) analysis [55] using DFT method to give clear evidence of stabilization originating from various molecular interactions. The hyperconjugative interaction energy was deduced from the second-order perturbation approach [56]

$$E(2) = \Delta E_{ij} = q_i \frac{F(i,j)^2}{\varepsilon_j - \varepsilon_i}$$

where q_i is the donor orbital occupancy, ε_i and ε_j are diagonal elements and $F(i,j)$ is the off diagonal NBO Fock matrix element.

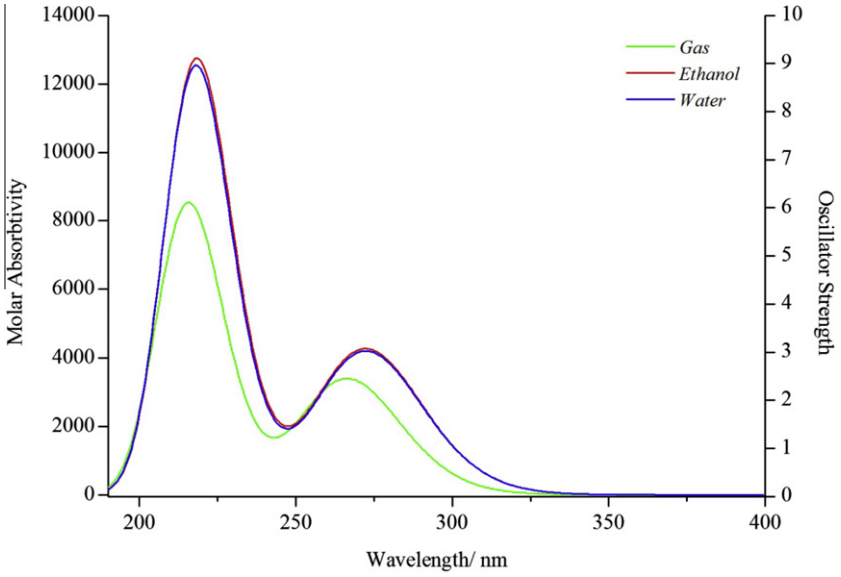

Fig. 9. Theoretical UV spectra of 2A4Cl6MP.

NBO analysis provides an efficient method for studying intra and intermolecular bonding and interaction among bonds, and also provides a convenient basis for investigating charge transfer of conjugative interaction in molecular systems [57].

The larger the $E(2)$ value, the more intensive is the interaction between electron donors and electron acceptors, i.e. the more donating tendency from electron donors to electron acceptors and the greater the extent of conjugation of the whole system. In our title molecule, the intramolecular hyperconjugative interactions are formed by the orbital overlap between bonding (C—C) and (N—C) and anti-bonding (C—C), (N—C) and (C—H) orbital which results in intramolecular charge transfer (ICT) causing stabilization of the molecular system. These interactions are observed as an increase in electron density (ED) in C—C, (N—C) and (C—H) antibonding orbital that weakens the respective bonds. The electron density of conjugated double bond of pyrimidine (~1.66e) clearly demonstrates strong delocalization as evident from Table 5. The intramolecular hyperconjugative interactions of the π–π^* transitions from [N1–C2 → N3–C4(7.74), C5–C6(35.10); N3–C4 → N1–C2(30.20), C5–C6(7.62); C5–C6 → N1–C2(10.83), N3–C4(37.96)] π bonds in pyrimidine ring lead to strong delocalization. As well as the hyperconjugative interactions of the $\sigma \rightarrow \sigma^*$ transitions occur from various bonds in our molecule. Particularly, σ (N1–C2), (N1–C6), (C2–N3), (N3–C4) and (C5–C6) having the bigger energetic contribution of their antibonding σ^* (C6–C12), (C2–N9), (C4–Cl), (C2–N9) and (C4–C18) interactions at 3.78, 3.62, 5.97, 3.17 and 5.49 kJ/mol, respectively. The most interaction energy, related to the resonance in the molecule, electron donating from the LP(1) N9 to the antibonding π^* (C1–C2) leads to moderate stabilization energy of 50.81 kJ/mol is shown in Table 5. In addition, the interactions are calculated at π^* (N1–C2) and (N3–C4) with π^* (C5–C6) shows enormous stabilization energy of 105.13 and 91.48 kJ/mol, respectively.

UV–Vis spectral analysis

The broad absorption bands associated to a strong $\pi \rightarrow \pi^*$ and a weak $\sigma \rightarrow \sigma^*$ transition characterize the UV–Vis absorption spectra. Natural bond orbital analysis indicates that molecular orbitals are mainly composed of σ and π atomic orbitals. The electronic absorption spectra of the title compound in ethanol and water as solvents were recorded within the 200–400 nm range and representative spectra are shown in Fig. 8. As can be seen from the Fig. 8, electronic absorption spectra showed three bands at 277.5, 232.0 and 202.0 nm for ethanol and at 292.5, 229.5 and 196 nm for water. Electronic absorption spectra were calculated using the TD-DFT method based on the B3LYP/6-311++G(d,p) level optimized structure in gas phase. The calculated results are listed in Table 6 along with the experimental absorption spectral data. For the TD-DFT calculations, the theoretical absorption bands are predicted at 266.6, 264.3, 228.4, 222.3, 215.3 and 208.2 nm in gas phase. TD-DFT calculations of the title compound in ethanol and water as solvent were performed using the PCM model. Thus, from TD-DFT calculation, the theoretical absorption bands are predicted at 272.9, 222.7 and 208.2 nm in ethanol medium and can easily be seen that they correspond well with the experimental data. The theoretically predicted UV spectra by TD-DFT level are shown in Fig. 9.

Frontier molecular orbital analysis

The total energy, energy gap and dipole moment affect the stability of a molecule. Surfaces for the frontier orbital were drawn to understand the bonding scheme of present compound and it is shown in Fig. 10. The conjugated molecules are characterized by a highest occupied molecular orbital-lowest unoccupied molecular orbital (HOMO–LUMO) separation, which is the result of a significant degree of intermolecular charge transfer (ICT) from the end-capping electron-donor to the efficient electron acceptor group through π-conjugated path. The HOMO is the orbital that primarily acts as an electron donor and the LUMO is the orbital that largely acts as the electron acceptor, and the gap between HOMO and LUMO characterizes the molecular chemical stability. The energy gap between the HOMO and the LUMO molecular orbitals is a critical parameter in determining molecular electrical transport properties because it is a measure of electron conductivity. The HOMO is delocalized over the entire molecule except methyl group. The HOMO → LUMO transition implies an electron density transfer to benzene ring and hydrogen atoms of methyl group through benzene ring from amino group. The computed energy values of HOMO

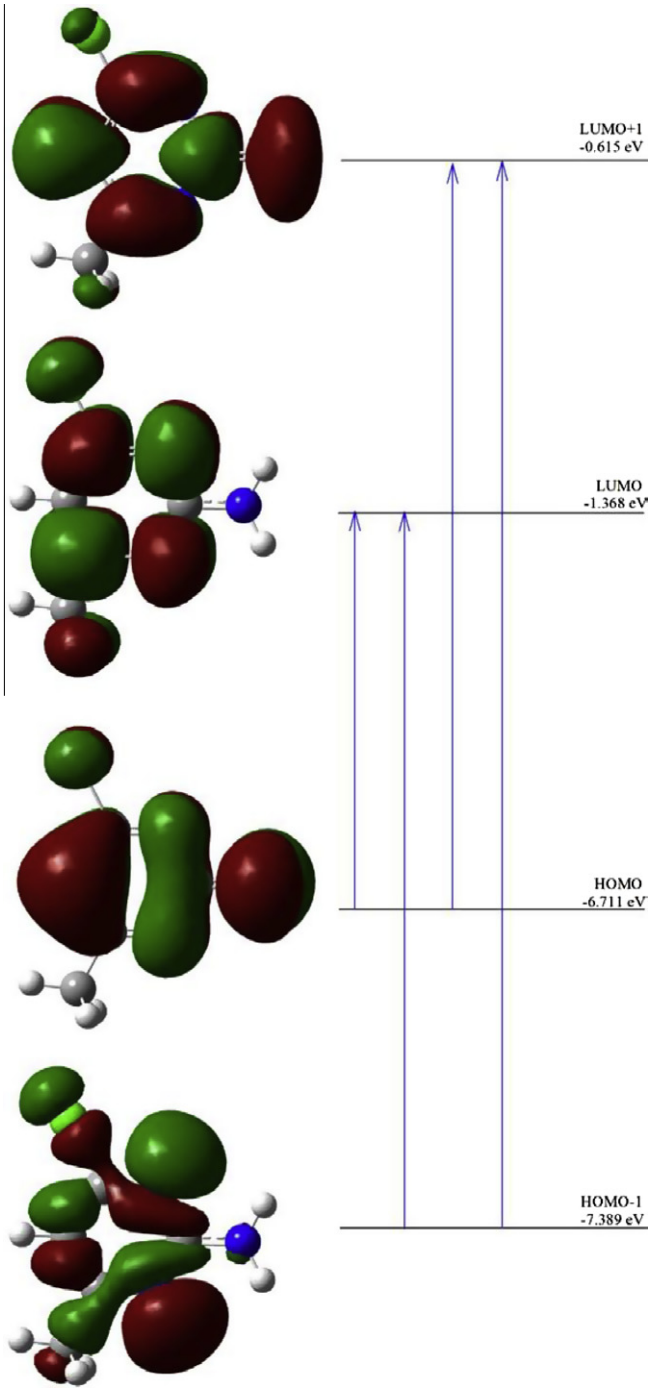

Fig. 10. Frontier molecular orbitals of 2A4Cl6MP in gas phase.

Table 7
Calculated energy values of 2A4Cl6MP in its ground state.

	Gas	Ethanol	Water
E_{Total} (Hartree)	−818.57798214	−818.58972002	−818.59013696
E_{LUMO+1} (eV)	−0.615	−0.653	−0.656
E_{LUMO} (eV)	−1.368	−1.480	−1.486
E_{HOMO} (eV)	−6.711	−6.739	−6.742
E_{HOMO-1} (eV)	−7.389	−7.575	−7.586
$\Delta E_{HOMO-LUMO}$ (eV)	5.343	5.259	5.256
$\Delta E_{HOMO-LUMO+1}$ (eV)	6.096	6.087	6.086
$\Delta E_{HOMO-1-LUMO}$ (eV)	6.021	6.095	6.099
$\Delta E_{HOMO-1-LUMO+1}$ (eV)	6.774	6.922	6.930
Chemical hardness (η)	2.671	2.630	2.628
Electronegativity (χ)	4.040	4.109	4.114
Chemical potential (V)	−4.040	−4.109	−4.114
Electrophilicity index (ω)	3.054	3.211	3.221
μ_x	2.163	2.597	2.611
μ_y	−0.228	−0.546	−0.570
μ_z	0.409	0.506	0.513
μ_{total}	2.213	2.701	2.721

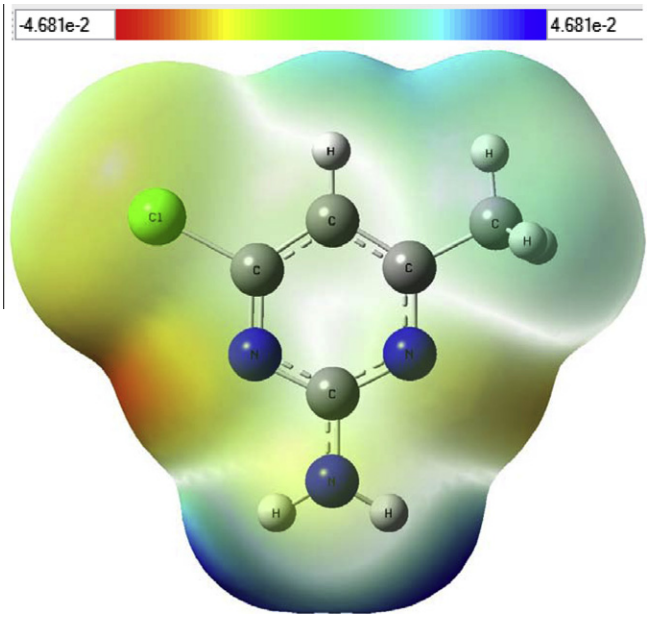

Fig. 11. Molecular electrostatic potential map of 2A4Cl6MP.

and LUMO in gas phase are −6.711 eV and −1.368 eV, respectively. The energy gap value is 5.343 eV for 2A4Cl6MP molecule. The energy values of the frontier orbitals are presented in Table 7. The energy gap between HOMO and LUMO determines the kinetic stability, chemical reactivity and, optical polarizability and chemical hardness–softness of a molecule [58].

Ionization potential

By using HOMO and LUMO energy values for a molecule, the ionization potential and chemical hardness of the molecule were calculated using Koopmans' theorem [59] and are given by

$\eta = (I_P - E_A)/2$ where $I_P \approx -E(HOMO)$, $E_A \approx -E(LUMO)$, I_P = Ionization potential (eV), E_A = electron affinity (eV),

$$\eta = \left[\frac{E(LUMO) - E(HOMO)}{2}\right]$$

The ionization potential of the 2-amino-4-chloro-6-methylpyrimidine in gas phase is 6.711 eV. The ionization potential calculated for same molecule in ethanol as medium is 6.739 eV. Considering the chemical hardness, large HOMO–LUMO gap means a hard molecule and small HOMO–LUMO gap means a soft molecule. One can also relate the stability of molecule to hardness, which means that the molecule with least HOMO–LUMO gap means it is more reactive.

Molecular electrostatic potential

The different values of the electrostatic potential at the surface are represented by different colors. Potential increases in the order

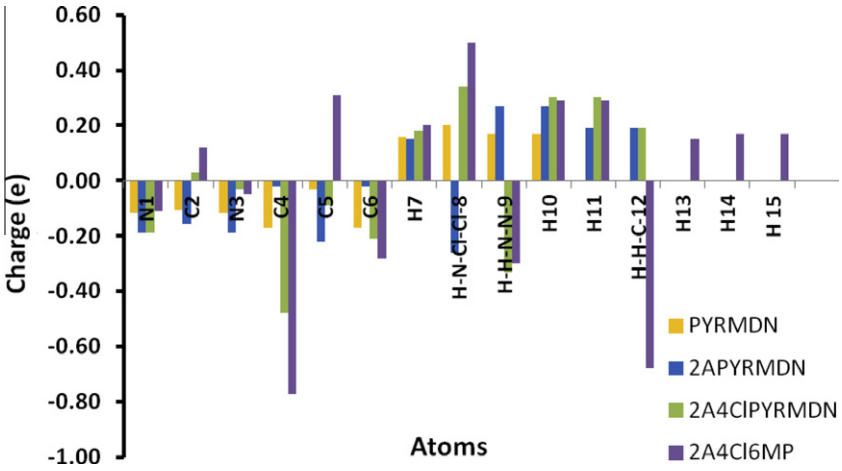

Fig. 12. The histogram of calculated Mulliken charge for 2A4Cl6MP.

Table 8
Mulliken atomic charges of 2A4Cl6MP calculated by DFT/B3LYP/6-311++G(d,p).

Atoms	PYRMDN[a]	2APYRMDN[b]	2A4ClPYRMDN[c]	2A4Cl6MP[d]
N1	−0.12	−0.19	−0.19	−0.11
C2	−0.10	−0.15	0.03	0.12
N3	−0.12	−0.19	−0.03	−0.05
C4	−0.17	−0.02	−0.48	−0.77
C5	−0.03	−0.22	−0.09	0.31
C6	−0.17	−0.02	−0.21	−0.28
H7	0.16	0.15	0.18	0.20
H–N–Cl–Cl–8	0.20	−0.26	0.34	0.50
H–H–N–N–9	0.17	0.27	−0.33	−0.30
H10	0.17	0.27	0.30	0.29
H11		0.19	0.30	0.29
H–H–C–12		0.19	0.19	−0.68
H13				0.15
H14				0.17
H 15				0.17

[a] PYRMDN: pyrimidine.
[b] 2APYRMDN: 2-amino-pyrimidine.
[c] 2A4ClPYRMDN: 2-amino-4-chloro-pyrimidine.
[d] 2A4Cl6MP: 2-amino-4-chloro-6-methylpyrimidine.

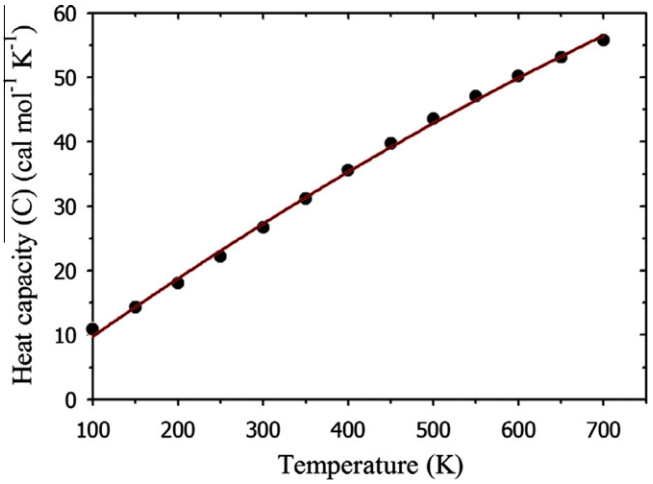

Fig. 13. Correlation graphic of heat capacity and temperature for 2A4Cl6MP.

Table 9
Thermodynamic properties at different temperatures at the B3LYP/6-311++G(d,p) level for 2A4Cl6MP.

T (K)	C (cal mol^{-1} K^{-1})	S (cal mol^{-1} K^{-1})	ΔH (kcal mol^{-1})
100	13.803	66.273	1.095
150	18.542	73.588	2.005
200	22.997	80.107	3.143
250	27.327	86.15	4.501
300	31.529	91.868	6.072
350	35.539	97.339	7.849
400	39.283	102.597	9.820
450	42.718	107.66	11.971
500	45.829	112.534	14.286
550	48.629	117.225	16.748
600	51.144	121.739	19.343
650	53.406	126.083	22.057
700	55.446	130.264	24.878

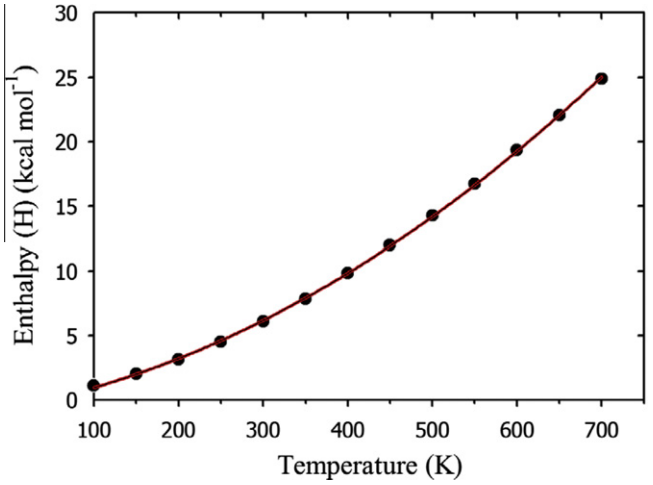

Fig. 14. Correlation graphic of enthalpy and temperature for 2A4Cl6MP.

red < orange < yellow < green < blue. The color code of these maps is in the range between −29.3737 kcal/mol (deepest red) to 29.3737 kcal/mol (deepest blue) in compound, where blue indicates the strongest attraction and red indicates the strongest repulsion. As can be seen from the MEP map of the title molecule, while regions having the negative potential are over the electronegative atom (nitrogen atoms), the regions having the positive potential are over the hydrogen atoms. The negative potential value is −24.5876 kcal/mol for nitrogen atom (in the ring, N3). A maximum positive region localized on the H atom bond has value of

+29.1986 kcal/mol (NH_2 for H atom, H10). From these results, we can say that the H atoms indicate the strongest attraction and O atom indicates the strongest repulsion. Fig. 11 provides a visual representation of the chemically active sites and comparative reactivity of the atoms.

Mulliken charge analysis

It is clear that Mulliken populations yield one of the simplest pictures of charge distribution and Mulliken charges render net atomic populations in the molecule. The charge distributions of 2-amino-4-chloro-6-methylpyrimidine have been calculated by B3LYP/6-311++G(d,p) level of theory and shown in Fig. 12. The results are given in Table 8. As can be seen from the Table 8, the magnitudes of the carbon atomic charges, found to be either positive or negative, were noted to change from −0.77 to 0.31. All the hydrogen atoms have a positive charge and all the nitrogen atoms have a negative charge. The chlorine atom has the maximum positive charge than the other atoms since it is an acceptor atom and C4 atom has a maximum negative charge since C4 is a donor atom.

Thermodynamic properties

On the basis of vibrational analysis, the statically thermodynamic functions: heat capacity (C), enthalpy changes (H) and entropy (S) for the title molecule were obtained from the theoretical harmonic frequencies and listed in Table 9. From the Table 9, it can be observed that these thermodynamic functions are increasing with temperature ranging from 100 to 700 K due to the fact that the molecular vibrational intensities increase with temperature. The correlation equations between heat capacity, enthalpy, entropy changes and temperatures were fitted by quadratic formulas and the corresponding fitting factors (R^2) for these thermodynamic properties are 0.9999, 0.9999 and 0.9998, respectively. The corresponding fitting equations are as follows and the correlation graphics of those shown in Figs. 13-15

$$C = 2.9931 + 0.1111T - 5.1444 \times 10^{-5} T^2 \quad (R^2 = 0.9999)$$
$$H = -0.5891 + 0.0120T + 3.5184 \times 10^{-5} T^2 \quad (R^2 = 0.9999)$$
$$S = 52.9777 + 0.1434T - 4.7623 \times 10^{-5} T^2 \quad (R^2 = 0.9998)$$

All the thermodynamic data supply helpful information for the further study on the 2A4Cl6MP. They can be used to compute the other thermodynamic energies according to relationships of thermodynamic functions and estimate directions of chemical reactions according to the second law of thermodynamics in Thermochemical field. Notice: all thermodynamic calculations were done in gas phase and they could not be used in solution.

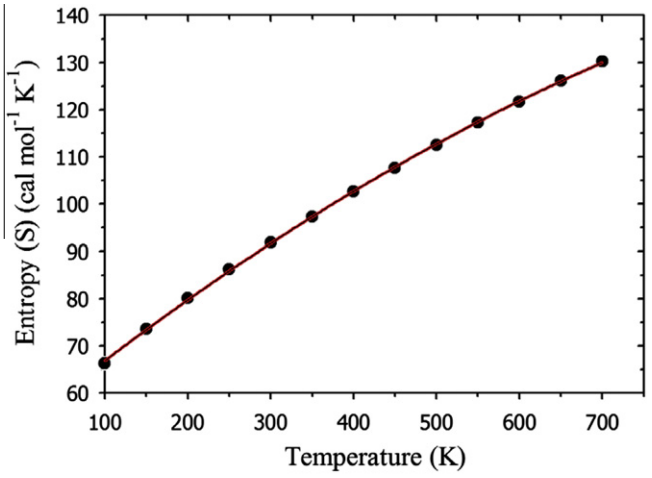

Fig. 15. Correlation graphic of entropy and temperature for 2A4Cl6MP.

Conclusions

The FTIR, FT-Raman, ^{1}H and ^{13}C NMR spectra, UV–Vis spectral measurements have been made for the 2A4Cl6MP molecule. The complete vibrational analysis and first order hyperpolarizability, NBO analysis, HOMO and LUMO analysis and thermodynamic properties of the title compound was performed on the basis of DFT calculations at the B3LYP/6-311++G(d,p) basis set. The consistency between the calculated and experimental FTIR and FT-Raman data indicates that the B3LYP/6-311++G(d,p) method can generate reliable geometry and related properties of the tile compound. The difference between the observed and scaled wavenumber values of most of the fundamentals is very small. The theoretically constructed FTIR and FT-Raman spectra exactly coincide with experimentally observed counterparts. The ^{1}H and ^{13}C NMR chemical shifts were calculated and compared with experimental one. The calculated dipole moment and first order hyperpolarizability results indicate that the title compound is a good candidate of NLO material. The UV spectrum was measured in water and ethanol solution and compared with theoretical values in gas phase and in ethanol environment (PCM model) using TD-DFT/6-311++G(d,p) basis set. Thermodynamic properties in the range from 100 to 700 K are obtained.

References

[1] N.H. Ouf, A.E.-G.E. Amr, Monatsh Chem. 139 (2008) 579–585.
[2] N. Neamati, Expert Opin. Investig. Drugs 12 (2003) 289–292.
[3] J. Sigmond, G.J. Peters, Nucleos Nucleot. Nucleic Acids 24 (2005) 1997–2022.
[4] J. Bolos, Mini. Rev. Med. Chem. 5 (2005) 857–868.
[5] T.J.J. Muller, R. Braun, M. Ansorge, Org. Lett. 2 (2002) 1967–1970.
[6] Z.H. Peng, M. Journet, G. Humphrey, Org. Lett. 8 (2006) 385–398.
[7] I. Collins, J. Chem. Soc. Perkin Trans. 1 (2000) 2845–2861.
[8] I. Collins, J. Chem. Soc. Perkin Trans. 1 (2002) 1921–1940.
[9] Gaussian Inc., Gaussian 03 Program, Gaussian Inc., Wallingford, 2004.
[10] A.D. Becke, J. Chem. Phys. 98 (1993) 5648–5652.
[11] A.D. Becke, J. Chem. Phys. 107 (1997) 8554–8560.
[12] C. Lee, W. Yang, C.R. Parr, Phys. Rev. B 37 (1988) 785–789.
[13] W.J. Hehre, L. Random, P.V.R. Schleyer, J.A. Pople, Ab Initio Molecular Orbital Theory, Wiley, New York, 1989.
[14] R. Dennington II, T. Keith, J. Millam, Gauss View, Version 4.1.2, Semichem, Inc., Shawnee Mission, KS, 2007.
[15] M.H. Jamróz, Vibrational Energy Distribution Analysis VEDA 4, Warsaw, 2004.
[16] K. Wolonski, J.F. Hinton, P. Pulay, J. Am. Chem. Soc. 112 (1990) 8251–8260.
[17] G. Keresztury, S. Holly, J. Varga, G. Besenyei, A.Y. Wang, J.R. Durig, Spectrochim. Acta 9A (1993) 2007–2026.
[18] G. Keresztury, in: J.M. Chalmers, P.R. Griffith (Eds.), Raman Spectroscopy: Theory, Hand Book of Vibrational Spectroscopy, vol. 1, John Wiley & Sons Ltd., New York, 2002.
[19] W.-C. Guo, X.-H. Liu, P.-Q. Chen, H.-B. Song, Z.-M. Li, Chinese J. Struct. Chem. 9 (2007) 1005–1008.
[20] L.E. Sutton, Tables of Interatomic Distances, Chemical Society, London, 1958.
[21] N. Sundaraganesan, S. Illakiamani, H. Saleem, P.M. Wojciechowski, D. Michalska, Spectrochim. Acta 61A (2005) 2995–3001.
[22] N.B. Colthup, L.H. Daly, S.E. Wiberley, Introduction to Infrared and Raman Spectroscopy, third ed., Academic Press, Boston, 1990.
[23] N. Sundaraganesan, K. Satheshkumar, C. Meganathan, B.D. Joshua, Spectrochim. Acta 65A (2006) 1186–1196.
[24] R.A. Yadav, I.S. Sing, Ind. J. Pure Appl. Phys. 23 (1985) 626–627.
[25] K.B. Wiberg, A. Shrake, Spectrochim. Acta 29A (1973) 583–594.
[26] V. Krishnakumar, R. John Xavier, Spectrochim. Acta 63A (2006) 454–463.
[27] G. Yang, S. Matsuzono, E. Koyama, H. Tokuhisa, K. Hiratani, Macromolecules 34 (2001) 6545–6547.
[28] P. Pazderza, H. Divisova, H. Havilsova, P. Borek, Molecules 5 (2000) 189–194.
[29] P. Pazderza, H. Divisova, H. Havilsova, P. Borek, Molecules 5 (2000) 1166–1174.
[30] H. Arslan, U. Florke, N. Kulcu, G. Binzet, Spectrochim. Acta 68A (2007) 1347–1355.
[31] P.M. Wojciechowski, D. Michalska, Spectrochim. Acta A 68 (2007) 948–955.
[32] G. Socrates, Infrared Characteristic Group Frequencies, Wiley-Interscience Publications, New York, 1980.
[33] N. Sandhyarani, G. Skanth, S. Berchmans, V. Yegnarman, T. Pradeep, J. Colloid Interface Sci. 209 (1999) 154–163.

[34] P.L. Anto, C.Y. Panicker, H.T. Varghese, D. Philip, O. Temiz-arpaci, B.T. Gulbas, I. Yildiz, Spectrochim. Acta 67A (2007) 744–749.
[35] K.R. Ambujakshan, V.S. Madhavan, H.T. Varghese, C.Y. Panicker, O. Temiz-arpaci, B. T Gulbas, I. Yildiz, Spectrochim. Acta 69A (2008) 782–788.
[36] N. Sundaraganesan, B.D. Joshua, C. Meganathan, S. Sebastian, Ind. J. Chem. 47 (2008) 821–829.
[37] D. Sajan, I. Hubert Joe, V.S. Jayakumar, J. Raman Spectrosc. 37 (2005) 508–519.
[38] M. Gussoni, C. Castiglioni, M.N. Ramos, M.C. Rui, G. Zerbi, J. Mol. Struct. 224 (1990) 445–470.
[39] J.F. Arenas, I. Tocon, J.C. Otero, J.I. Marcos, J. Mol. Struct. 410–411 (1997) 443–446.
[40] B.V. Reddy, G.R. Rao, Vib. Spectrosc. 6 (1994) 231–250.
[41] D.A. Long, W.O. Jeorge, Spectrochim. Acta 19 (1963) 1777–1790.
[42] M. Dien, Introduction to Modern Vibrational Spectroscopy, Wiley, New York, 1993.
[43] H.O. Kalinowski, S. Berger, S. Braun, Carbon-13 NMR Spectroscopy, John Wiley & Sons, Chichester, 1988.
[44] K. Pihlaja, E. Kleinpeter (Eds.), Carbon-13 Chemical Shifts in Structural and Sterochemical Analysis, VCH Publishers, Deerfield Beach, 1994.
[45] Y.X. Zhao, X.Y. Sun, Spectroscopic Identification of Organic Structures, Science Press, 2010. 278.
[46] Y.X. Sun, Q.L. Hao, W.X. Wei, Z.X. Yu, L.D. Lu, X. Wang, Y.S. Wang, J. Mol. Struct.: Theochem. 904 (2009) 74–82.
[47] C. Andraud, T. Brotin, C. Garcia, F. Pelle, P. Goldner, B. Bigot, A. Collet, J. Am. Chem. Soc. 116 (1994) 2094–2102.
[48] V.M. Geskin, C. Lambert, J.L. Bredas, J. Am. Chem. Soc. 125 (2003) 15651–15658.
[49] M. Nakano, H. Fujita, M. Takahata, K. Yamaguchi, J. Am. Chem. Soc. 124 (2002) 9648–9655.
[50] D. Sajan, I.H. Joe, V.S. Jayakumar, J. Zaleski, J. Mol. Struct. 785 (2006) 43–53.
[51] D.A. Kleinman, Phys. Rev. 126 (1962) 1977–1979.
[52] C. Jesintha John, M. Amalanathan, D. Sajan, K. Udaya Lakshmi, I.H. Joe, Spectrochim. Acta 78A (2011) 264–272.
[53] M.C. Ruiz Delgado, V. Hernandez, J. Casado, J.T. Lopez Navarre, J.M. Raimundo, P. Blanchard, J. Roncali, J. Mol. Struct. 151 (2003) 651–653.
[54] J.P. Abraham, D. Sajan, V. Shettigar, S.M. Dharmaprakash, I. Nemec, I.H. Joe, V.S. Jayakumar, J. Mol. Struct. 917 (2009) 27–36.
[55] H.W. Thomson, P. Torkington, J. Chem. Soc. 171 (1945) 640–645.
[56] E.D. Glendening, J.K. Badenhoop, A.E. Reed, J.E. Carpenter, J.A. Bohmann, C.M. Morales, F. Weinhold, NBO 5.0, Theoretical Chemistry Institute, University of Wisconsin, Madison, 2001.
[57] M. Snehalatha, C. Ravikumar, I.H. Joe, N. Sekar, V.S. Jayakumar, Spectrochim. Acta A 72 (2009) 654–662.
[58] B. Kosar, C. Albayrak, Spectrochim. Acta 78A (2011) 160–167.
[59] T.A. Koopmans, Physica 1 (1934) 104–113.